NUMERICAL SIMULATION OF KINETIC EFFECTS IN LOW-DENSITY HYPERSONIC AERODYNAMICS

Vladimir V. Riabov
Rivier College, Nashua, New Hampshire 03060, USA

Keywords: *DSMC, aerodynamic coefficients, hypersonic flows, toroidal ballute, spinning cylinder*

Abstract

The Direct Simulation Monte-Carlo technique (DSMC) is used for numerical analysis of rarefied-gas hypersonic flows near a blunt plate, wedge, two side-by-side plates and cylinders, sphere, torus, and rotating cylinder. Important kinetic effects that are specific for the transition flow regime have been found: non-monotonic lift of plates, strong repulsive force between side-by-side plates and cylinders, dependence of drag on torus radii ratio, and reverse Magnus effect on the lift of a rotating cylinder. The numerical results are in a good agreement with experimental data, which were obtained in a vacuum chamber at low and moderate Knudsen numbers from 0.01 to 10.

1 Introduction

Stimulated by planetary exploration programs [1], numerical and experimental studies [1-7] of aerodynamics of simple shape bodies have provided valuable information related to physics of rarefied-gas flows about spacecraft elements, testing devices, and in micro-channels. Numerous results were found in the cases of plates, wedges, cones, spheres, and cylinders [4-13].

In the present paper, hypersonic rarefied-gas flows about a blunt plate, wedge, disk, two side-by-side cylinders and plates, toroidal ballute, sphere, and spinning cylinder have been studied. The role of rarefaction parameter (Knudsen number), specific heat ratio, spinning rates, dissociation, surface temperature, and geometrical factors is investigated.

2 The Direct Simulation Monte-Carlo (DSMC) Method

The DSMC method [2] and DS2G code [14] are used in this study as a numerical technique for simulating low-density gas flows. Molecular collisions in air, oxygen, helium, and argon are modeled using the variable hard sphere (VHS) model [2]. The gas-surface interactions are assumed to be fully diffusive with full moment and energy accommodation. The DSMC/DSG2 code validation [9] was tested in comparing numerical results with experimental data [6-8] related to the simple-shape bodies.

3 Aerodynamics of a Blunt Plate

The comparison of the DSMC recent numerical results for a drag coefficient of a parallel plate (thickness $\delta = 0.1L$) with experimental data [7] in air (specific heat ratio $\gamma = 1.4$) is studied for Knudsen numbers $Kn_{\infty,L}$ from 0.02 to 3.2, Mach number $M_\infty = 10$, and temperature factor $t_w = T_w/T_0 = 1$. Numerical results correlate well with experimental data at $0.02 < Kn_{\infty,L} < 1$. The free-molecular limit [3] is approached at $Kn_{\infty,L} > 3$.

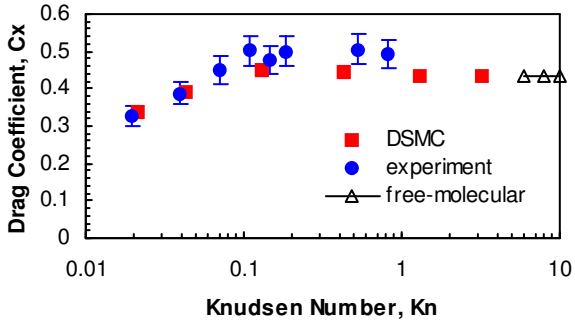

Fig. 1 Total drag coefficient of the plate vs. Knudsen number $Kn_{\infty,L}$ in air at $M_\infty = 10$ and $\alpha = 0$.

The study of the influence of Mach number M_∞ on the aerodynamic characteristics of bodies of simple shape has been conducted at moderate values of the Knudsen number and at constant values of similarity parameters: $Kn_{\infty,L}$, t_w, and γ. The regime of hypersonic stabilization [9] will occur at $M_\infty\theta >> 1$ in the case of streamlining of the thin bodies when the angle θ between the generatrix of the body surface and the direction of the upstream flow becomes small enough. This regime will be realized at smaller values of M_∞, if the angle θ increases.

The results of previous studies [6-8] indicate that the hypersonic flow independency principle [9] is realized in the transitional rarefied flow regime at $K = M_\infty \times \sin\theta > 1$. As was found in experiments [6-8], this principle is not true for thin bodies at small angles of attack in rarefied gas flows under the conditions $K < 1$.

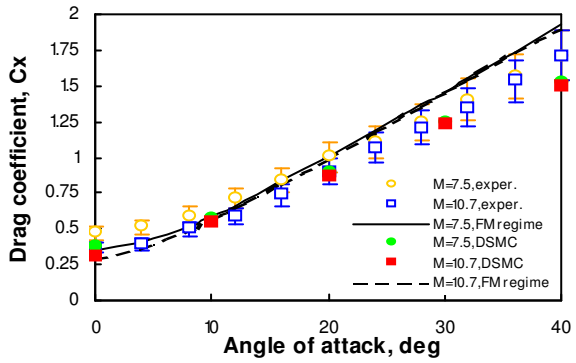

Fig. 2 Drag coefficient C_x for a blunt plate ($\delta = 0.06L$) at $Kn_{\infty,L} = 0.6$ and $M_\infty = 7.5$ (circles) and 10.7 (squares) in helium. Experimental data from Refs. 6-8.

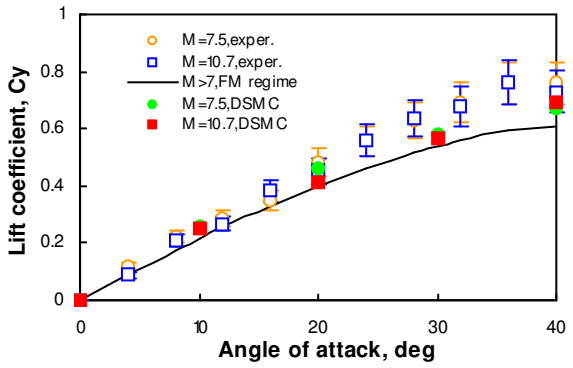

Fig. 3 Lift coefficient C_y for a blunt plate ($\delta = 0.06L$) at $Kn_{\infty,L} = 0.6$ and $M_\infty = 7.5$ (circles) and 10.7 (squares) in helium. Experimental data from Refs. 6-8.

The drag coefficient of a blunt plate having relative thickness $\delta = 0.06L$ becomes sensitive to the magnitude of the freestream Mach number in helium flow (Fig. 2, $M_\infty = 7.5$ and $M_\infty = 10.7$) at small angles of attack $\alpha < 12$ deg. The results calculated by the DSMC technique (filled markers) correlate well with the experimental data [6-8] (empty markers). For the lift coefficient, the free-molecular flow data [3], as well as computational and experimental results presented in Fig. 3, are independent of the Mach number, and the value $C_{y,FM}$ is less by approximately 15% than the value C_y for transitional flow regime at $\alpha > 16$ deg. This phenomenon was discussed in Ref. 9.

The temperature factor is other important similarity parameter [4-9], which effects pressure at the body surface. Numerical data for a plate ($\delta = 0.1L$) at angle attack $\alpha = 20$ deg and various $Kn_{\infty,L}$ has been studied (Figs. 4-5).

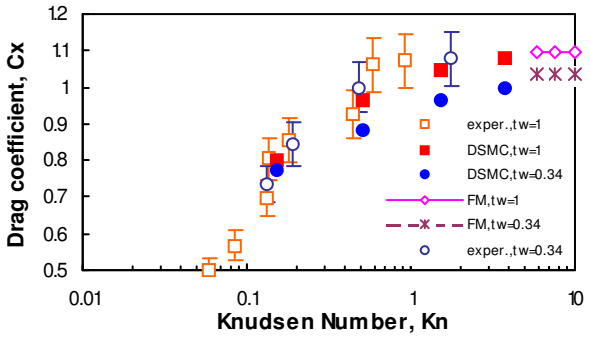

Fig. 4 Drag coefficient C_x for a blunt plate ($\delta = 0.1L$; $\alpha = 20$ deg) in air vs. Knudsen number $Kn_{\infty,L}$ at various temperature factors t_w. Experimental data from Ref. 7.

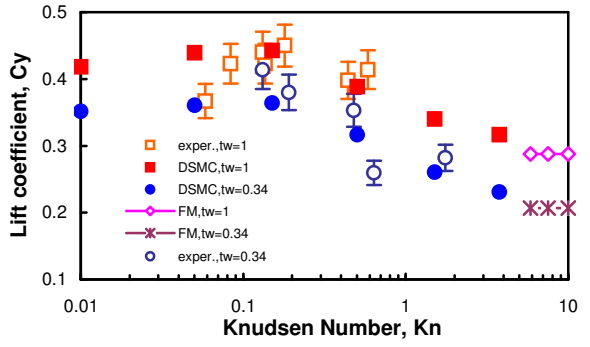

Fig. 5 Lift coefficient C_y for a blunt plate ($\delta = 0.1L$; $\alpha = 20$ deg) in air vs. Knudsen number $Kn_{\infty,L}$ at various temperature factors t_w. Experimental data from Ref. 7.

The lift coefficient, C_y (see Fig.5) changes non-monotonically from the continuum to the free-molecular flow regime. Maximum values occur in the transitional flow regime. The

influence of t_w can be estimated as 25% for C_y. The results correlate well with the experimental data [7].

4 Aerodynamics of a Wedge

The dependence of drag and lift coefficients for a wedge (θ = 20 deg) on the angle of attack has been studied in numerical simulations of helium flow at $Kn_{\infty,L}$ = 0.3, t_w = 1, and the freestream Mach number M_∞ = 11.8. The DSMC results (squares) are shown in Figs. 6 and 7 for drag and lift coefficients, correspondingly. The base area of the wedge and its length were taken as the reference area and length.

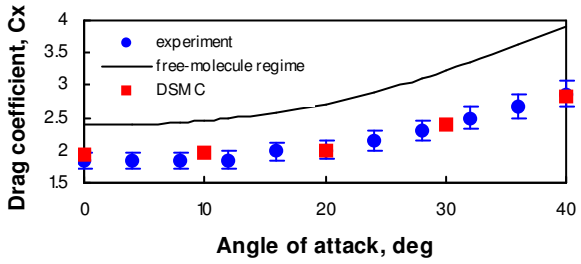

Fig. 6 Drag coefficient for a wedge (θ = 20 deg) in helium flow at $Kn_{\infty,L}$ = 0.3 and M_∞ = 11.8. Experimental data from Refs. 6-9.

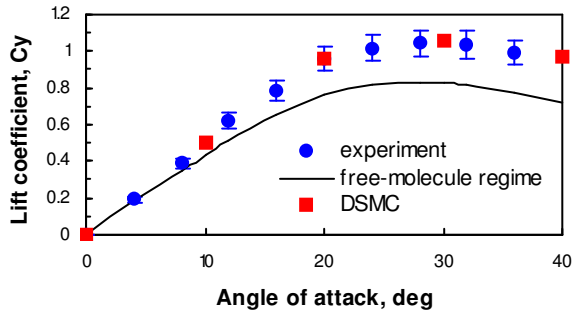

Fig. 7 Lift coefficient for a wedge (θ = 20 deg) in helium flow at $Kn_{\infty,L}$ = 0.3 and M_∞ = 11.8. Experimental data from Refs. 6-9.

The numerical results correlate well with the experimental data [6-9] (circles), which were obtained in a vacuum wind tunnel at the same flow parameters. In both transitional and free-molecular [3] regimes, the characteristics are not sensitive to changes in upstream flow parameters at $M_\infty > 9$. Another interesting fact is that the lift-drag ratio in the transitional flow regime is larger by 50% than the corresponding parameter in the free-molecular regime (see, also, Refs. 5-9).

5 Aerodynamics of a Disk

In the free-molecular flow regime, the influence of the specific heat ratio γ on the aerodynamic characteristics of bodies depends on the normal component of the momentum of the reflected molecules, which is a function of γ [7-9]. The same phenomenon can be observed at the transitional conditions in the case of the disk at α = 90 deg. The nitrogen-argon pair was the most acceptable one for testing [6-9]. The dependencies of C_x of the disc for Ar (filled triangles) and N_2 (filled squares) are shown in Fig. 8 for a wide range of Knudsen numbers ($Kn_{\infty,D}$). At the same parameters of the upstream flow, numerical data obtained by the DSMC technique for different models of molecules are compared with experimental data [6-8].

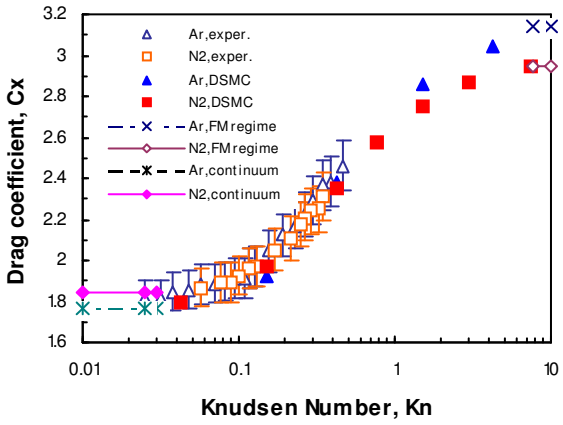

Fig. 8 Drag coefficient C_x for a disk (α = 90 deg) vs. Knudsen number $Kn_{\infty,D}$ in argon (triangles) and nitrogen (squares). Experimental data from Refs. 6-8.

The influence of specific heat ratio on the drag coefficient is more significant for large values of $Kn_{\infty,D} > 1$. In the free molecular regime ($Kn_{\infty,D} > 7$) an increase of C_x is observed as γ increases [3, 9]. This increase is caused by the dependence on γ of the reflected momentum of the molecules at t_w = 1. The degree of this influence has been evaluated as 8% at $Kn_{\infty,D} > 2$. As the number $Kn_{\infty,D}$ decreases, this influence decreases, and at $Kn_{\infty,D} < 0.4$, the drag coefficient of the disk in diatomic gas becomes

larger than that for a monatomic gas. In the continuum flow regime, the dependence of the drag-coefficient on γ difference is insignificant.

6 Heat Flux on a Sphere

The values of the Stanton numbers *St* at the stagnation point of a sphere were calculated by the DSMC method [15] (squares) under wind-tunnel conditions at various Knudsen numbers, Mach number M_∞ = 15, and temperature factor t_w = 0.15 (see Fig. 9). The results correlate well with experimental data [16-19] (circles). The comparison of the data with the results from the thin viscous shock layer (TVSL) model (triangles) [20, 21] and the solutions of the full system of the Navier-Stokes equations with slip boundary conditions (empty diamonds) [22] indicates that the continuum models could not be properly applied at $Kn_{\infty,R} > 0.2$.

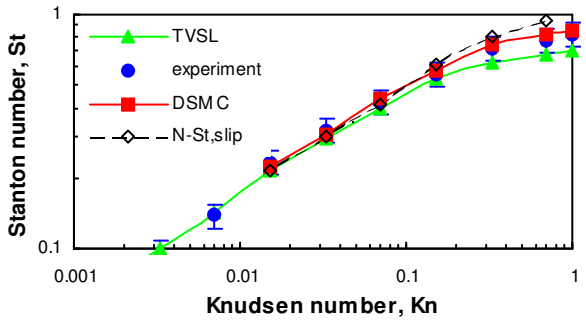

Fig. 9 Stanton numbers *St* for a sphere vs. Knudsen numbers $Kn_{\infty,R}$ for different medium models at various wind-tunnel experimental conditions [16-19].

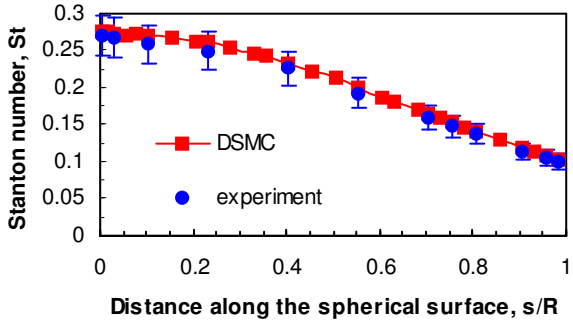

Fig. 10 Stanton numbers *St* along the spherical surface coordinate *s/R* at $Kn_{\infty,R}$ = 0.033, M_∞ = 6.5, t_w = 0.31. Experimental data from Refs. 16 and 23.

A comparison between the numerical data obtained by the DSMC method [15] (squares) and experimental data [16, 23] (circles) along the spherical surface is shown in Fig. 10. The parameters of upstream perfect gas flow were the following: $Kn_{\infty,R}$ = 0.033, M_∞ = 6.5, t_w = 0.315, and γ = 1.4.

7 Aerodynamics of Two Side-by-Side Plates

The flow pattern over two side-by-side plates is sensitive to the geometrical parameter, *H/L*, where 2*H* is a distance between the plates. The influence of this parameter on the flow structure has been studied for hypersonic flow of argon at M_∞ = 10, t_w = 1, and $0.024 \le Kn_{\infty,L} \le 1.8$.

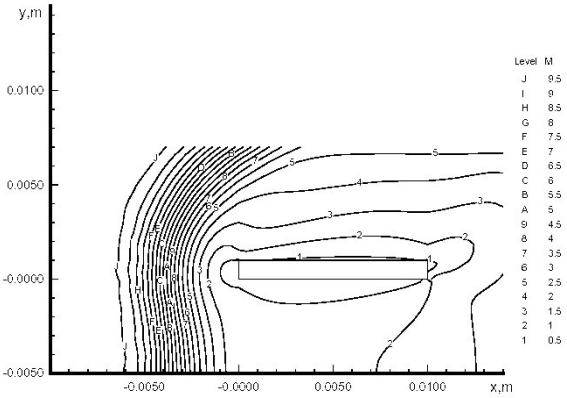

Fig. 11 Mach number contours in argon flow about a side-by-side plate at $Kn_{\infty,L}$ = 0.024 and *H/L* = 0.5.

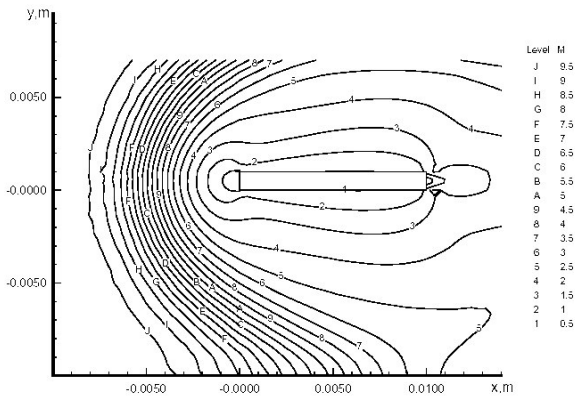

Fig. 12 Mach number contours in argon flow about a side-by-side plate at $Kn_{\infty,L}$ = 0.024 and *H/L* = 1.

At $H \le 0.5L$ (Fig. 11), the flow area between two side-by-side plates and cylinders becomes subsonic [7]. At $H > 0.5L$ (Fig. 12), two oblique shock waves interact in the vicinity of the symmetry plane generating the normal shock wave and the Mach reflected waves far behind the bodies.

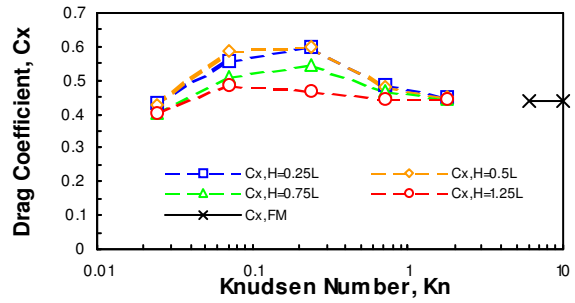

Fig. 13 Drag coefficient C_x of the side-by-side plates vs. Knudsen Number $Kn_{\infty,L}$ at $M_\infty = 10$.

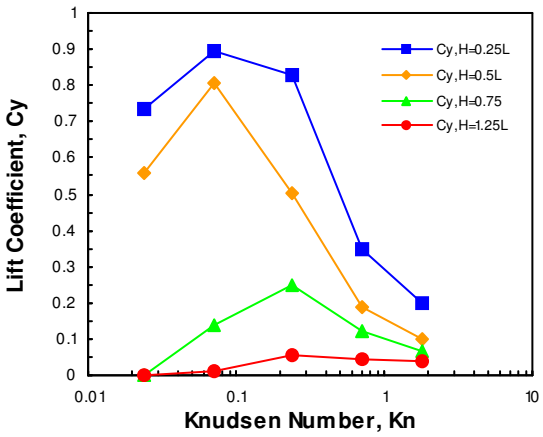

Fig. 14 Lift coefficient C_y of the side-by-side plates vs. Knudsen Number $Kn_{\infty,L}$ at $M_\infty = 10$.

Numerical results for the total drag and lift coefficients are also studied (see Figs. 13-14). The drag coefficient increases with Knudsen number, reaches a maximum, and then decreases to the free-molecular value [3]. The geometrical factor becomes insignificant as to its influence on the drag as both the continuum and free-molecule flow regimes are approached.

The repulsive lift force becomes significant at $H/L \le 0.75$, with the average lift-drag ratio of 1.6 for plates in the transition regime [10]. The rarefaction effects are responsible for non-monotonic dependency of the lift on the Knudsen number at $1.25 \ge H/L \ge 0.25$.

8 Aerodynamics of Two Side-by-Side Cylinders

The flow pattern over two side-by-side cylinders is also sensitive to the major geometrical similarity parameter, H/R (see Figs. 15 and 16), where $2H$ is a distance between the centers of the cylinders. The influence of this parameter on the flow structure has been studied for hypersonic flow of argon at $M_\infty = 10$ and $Kn_{\infty,R} = 0.1$.

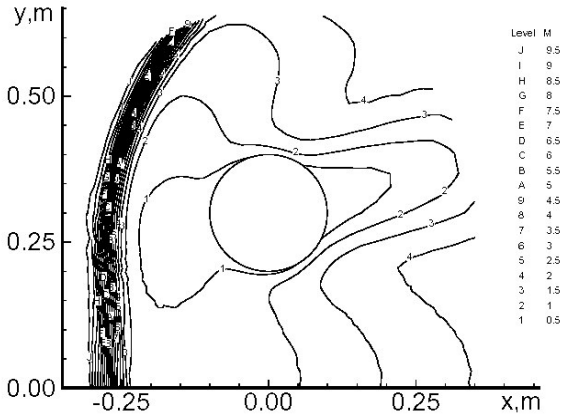

Fig. 15 Mach number contours in argon flow about a side-by-side cylinder at $Kn_{\infty,R} = 0.1$ and $H/R = 2$.

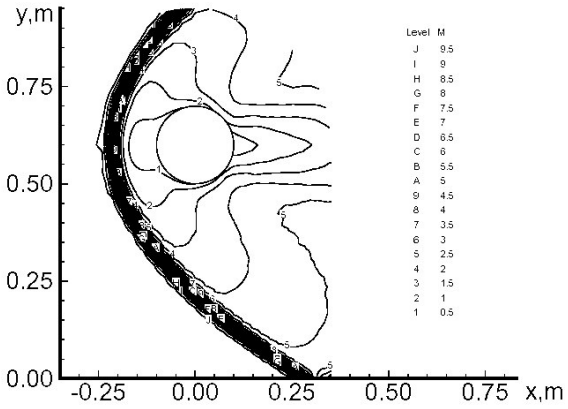

Fig. 16 Mach number contours in argon flow about a side-by-side cylinder at $Kn_{\infty,R} = 0.1$ and $H/R = 6$.

At the small ratio parameters, $H/R \le 2$ (see Fig. 15), the front shock-wave shape becomes normal, and front stagnation points relocate from the cylinder front zone towards the "throat" area [24]. This phenomenon effects the drag, pressure and skin-friction distributions along a cylinder and produces significant repulsive lift force (see Fig. 17) with $C_y/C_x = 0.35$. The geometrical factor becomes insignificant on the drag both under continuum flow regime conditions and in free-molecule flow at $H/R \ge 4$ (see Fig. 18).

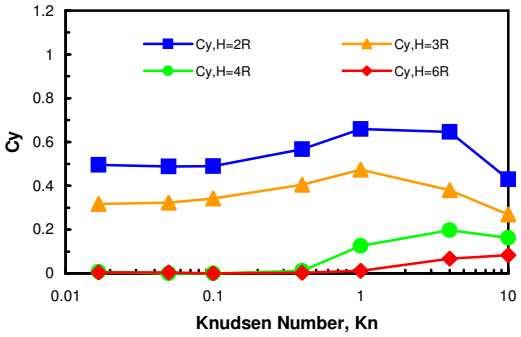

Fig. 17 Lift coefficient C_y of the side-by-side cylinder vs. Knudsen Number $Kn_{\infty,R}$ at $M_\infty = 10$.

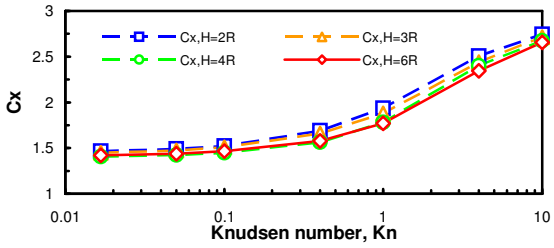

Fig. 18 Drag coefficient C_x of the side-by-side cylinder vs. Knudsen Number $Kn_{\infty,R}$ at $M_\infty = 10$.

9 Aerodynamics of a Torus

Strong influences of the geometrical factor, H/R (ratio of the distance between the axis of symmetry and the torus disk center H, and the torus radius R) and the Knudsen number, $Kn_{\infty,R}$ on the flow structure near a torus (the shape of shock waves and the stagnation point location), skin friction, pressure distribution, heat flux, and drag have been found. The influence of these parameters on the flow structure has been studied in argon at $M_\infty = 10$, $2R \le H \le 8R$, and $0.0167 \le Kn_{\infty,R} \le 10$.

At values of the parameter $H/R > 6$, the conical shock waves interact in the vicinity of the flow symmetry axis, creating the Mach disk. The reflected conical wave has a different pattern of the interaction with the supersonic flow behind a torus in continuum and rarefied flow regimes [11]. At $H/R > 8$, the flow near a torus is similar to that one about two side-by-side cylinders [24].

At smaller values of the parameter $H/R \le 4$, the shape of a front shock wave becomes normal, and the subsonic area is restricted by the location of the shock wave and the torus throat [11]. This "chocked-flow" effect plays a fundamental role in the redistribution of pressure and skin friction along the torus surface. The location of the stagnation-point ring (estimated through distributions of pressure and skin-friction coefficients) is moving from the front area to the torus throat after reducing the outer torus radius, H.

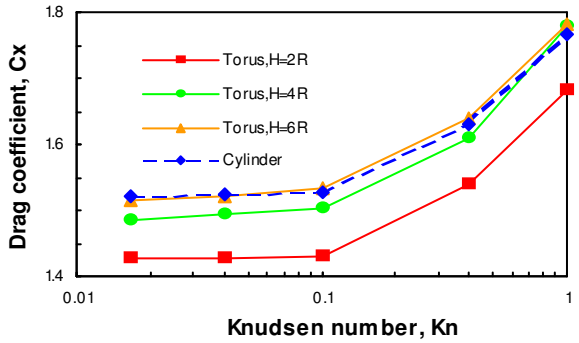

Fig. 19 Drag coefficient C_x of a spinning cylinder vs. Knudsen number Kn_D at M_∞ = 0.15 and different geometrical factors H/R in argon.

Numerical results of the total drag coefficient of a torus are also studied (see Fig. 19). The drag coefficient increases with increasing the Knudsen number. The geometrical factor becomes insignificant on the drag at $H/R \ge 6$ under continuum and free-molecule flow regimes.

10 Aerodynamics of a Toroidal Ballute

Aerocapture with large inflatable decelerators known as ballutes [25] is currently viewed as the most promising technology for a number of NASA's future robotic missions to Venus, Saturn, Titan, and Neptune [26-28]. The hypersonic flows of oxygen near a toroidal ballute model have been investigated numerically with the DSMC technique [11, 14] under transitional rarefied conditions (Knudsen numbers $Kn_{\infty,R}$ from 0.01 to 1).

The effect of dissociation on chocking of ducted flows has been studied numerically for a ballute model with varying area ratio H/H_*. The present study confirms the hypothesis [29] that the flow of dissociating gas (oxygen) (Fig. 20) is not choked at the "designed" toroid with a

throat radius H_* = 0.014 m., but the flow of perfect gas (Fig. 21) is choked at the similar conditions. The following parameters were used in calculations: $Kn_{\infty,R}$ = 0.01, R = 0.003 m, U_∞ = 5693 m/s, p_∞ = 1.28 kPa, and T_∞ = 1415 K.

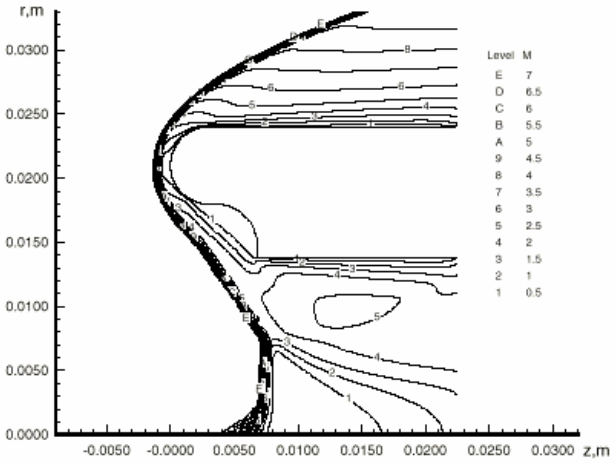

Fig. 20 Mach number contours in dissociating oxygen flow about a toroidal ballute model at $Kn_{\infty,R}$ = 0.01.

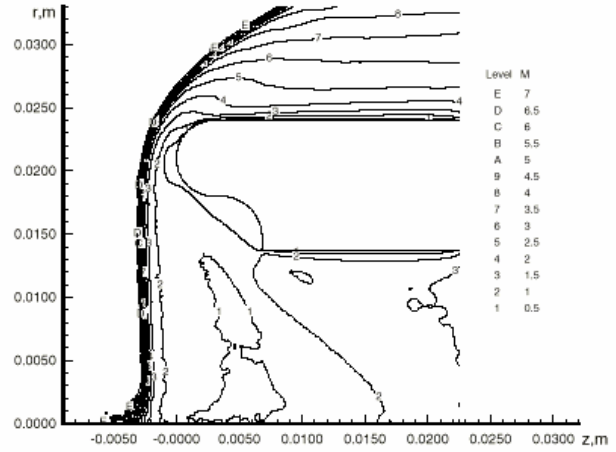

Fig. 21 Mach number contours in perfect-oxygen flow about a toroidal ballute model at $Kn_{\infty,R}$ = 0.01.

11 Aerodynamics of a Rotating Cylinder

At subsonic flow conditions, the speed ratio $S = M_\infty \cdot (0.5 \cdot \gamma)^{1/2}$ becomes small, and aerodynamic coefficients of a rotating cylinder become sensitive to the ratio magnitude [3, 12, 13]. The transition subsonic flow regime has been studied numerically in argon at M_∞ = 0.15 and spin ratio W = 1, 3, and 6. The lift and drag coefficients are shown in Figs. 22 and 23, respectively.

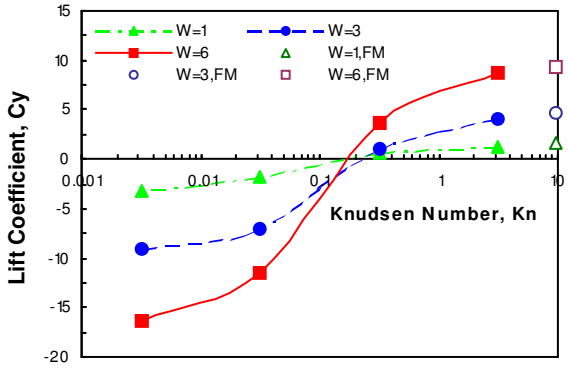

Fig. 22 Lift coefficient C_y of a spinning cylinder vs. Knudsen number Kn_D at M_∞ = 0.15 and different spin rates W in argon.

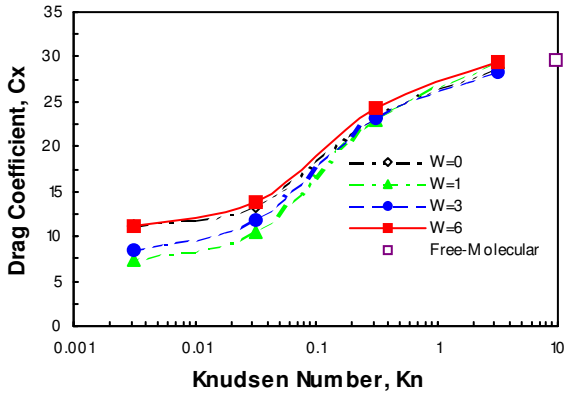

Fig. 23 Drag coefficient C_x of a spinning cylinder vs. Knudsen number Kn_D at M_∞ = 0.15 and different spin rates W in argon.

In the transition flow regime (Kn_D > 0.03), both the incident and reflected molecules significantly influence the lift [13]. The incident molecules dominate when Kn_D < 0.1, and the reflected molecules dominate when Kn_D > 0.1. The lift changes sign for the cylinder spinning in counter-clockwise direction. The drag becomes a slow function of the spin rate [12]. In the near-free-molecule flow regime (Kn_D = 3.18), the asymmetry of the flow in upper and bottom regions is significant [13]. The flow disturbances are concentrated in the vicinity of the spinning surface. In the near-continuum flow regime (Kn_D = 0.032), the circulating zone is much wider. These flow-pattern differences dominate the character of molecule-surface interactions.

The supersonic transition flow regime was investigated in [13, 30].

At supersonic flow conditions, the speed ratio S becomes large, and the aerodynamic coefficients become less sensitive to its magnitude [12, 13]. In the present study, the transition flow regime has been investigated numerically at $M_\infty = 10$, $\gamma = 5/3$ (argon gas), and spin ratio $W = 0.03$ and $W = 0.1$.

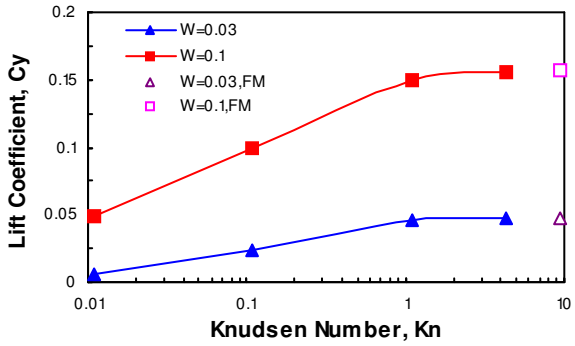

Fig. 24 Lift coefficient C_y of a spinning cylinder vs. Knudsen number Kn_D at M_∞ = 10 and different spin rates W in argon.

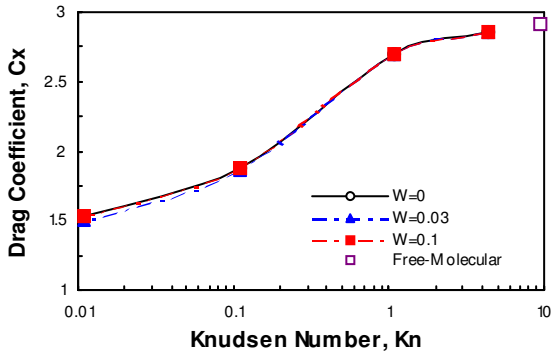

Fig. 25 Drag coefficient C_x of a spinning cylinder vs. Knudsen number Kn_D at M_∞ = 10 and different spin rates W in argon.

The lift and drag coefficients are shown in Figs. 24 and 25, respectively. For the lift coefficient, the influence of reflected molecules is dominant in the transition-flow regime ($Kn_D >$ 0.03). The incident-molecule input becomes significant at Knudsen number $Kn_D < 0.1$ [13]. Under the considered flow conditions, the lift coefficient has a positive sign (which is opposite to the sign under the continuum flow regime) for the cylinder spinning in a counter-clockwise direction. The drag coefficient is insensitive to the spin rate. The values of C_x and C_x at $Kn_D > 4$ are near the magnitudes of the coefficients for the free-molecule flow [3].

The flow characteristics are different in these cases [13]. For a small spin rate, W=0.1, the zone of circulating flow is located in the vicinity of the surface, and it does not affect the flow zone located far from the surface. The flow pattern becomes asymmetrical. The differences in flow patterns dominate the character of molecule-surface interactions, and they characterize the differences in the performance parameters under significantly distinct flow conditions (see Figs. 24 and 25).

12 Conclusions

The rarefied-gas flows about a blunt plate; wedge; two side-by-side plates and cylinders; sphere; torus; toroidal ballute, and spinning cylinder were studied by the DSMC technique. The effect of non-monotonic lift of plates in the transition flow regime has been studied. Both specific heat ratio and surface temperature factors affect significantly the lift. The lift-drag ratio for a wedge in the transitional flow regime is larger by 50% than the corresponding parameter in the free-molecular regime. The influence of specific heat ratio on the drag coefficient of a disk is significant (8%) for large values of Knudsen number.

The flow patterns near two side-by-side plates and cylinders are significantly different for small and large geometric factors. At $H/L \leq$ 0.5, the disturbances create a wide subsonic area, which occupies the "throat" area between the plates or cylinders. The rarefaction effects on the lift force are significant at $0.75 \geq H/L \geq$ 0.25, and they are responsible for non-monotonic dependency of the lift and drag forces of the plates.

The flow patterns near torus and ballute are also different for small and large inner-outer-radii ratios. At H/R = 2, the front shock-wave shape becomes normal, and the front stagnation points relocate towards the throat area. This phenomenon effects the drag, pressure and skin-friction distributions along the toroid. The present numerical study confirms the hypothesis [29] that the flow of dissociating gas (oxygen) is not choked at the "designed" toroidal ballute

model, but the flow of perfect gas is choked at the similar conditions.

The aerodynamic coefficients of a spinning cylinder have been evaluated for various Knudsen numbers and spin rates. At subsonic upstream conditions, the lift has different signs in the continuum and free-molecule flow regimes. The sign changes in the transitional flow regime (Kn_D = 0.1). The influential factors are magnitudes of momentum of the reflected and incident molecules, which depends on Kn_D.

A comparison of the results from various prediction methods (including numerical solutions of the full Navier-Stokes equations [22] and the Thin Viscous Shock Layer technique [20-21]) has been provided as well.

13 Acknowledgements

The author would like to express gratitude to G. A. Bird for the opportunity of using the DS2G computer program, V. N. Gusev and J. N. Moss for valuable discussions of the DSMC technique, and to I. Lourel for providing information about toroidal ballute models.

References

[1] Gnoffo P. Computational aerothermodynamics in aeroassist applications, *Journal of Spacecraft and Rockets*, Vol. 40, No. 3, pp. 305-312, 2003.

[2] Bird G. *Molecular gas dynamics and the direct simulation of gas flows.* 1st edition, Oxford University Press, 1994.

[3] Kogan M. *Rarefied gas dynamics*. New York: Plenum Press, 1969.

[4] Koppenwallner G and Legge H. Drag of bodies in rarefied hypersonic flow. *Thermophysical Aspects of Re-Entry Flows*, edited by C. Scott and J. Moss. Vol. 103, Progress in Astronautics and Aeronautics, Washington, DC: AIAA, pp. 44-59, 1994.

[5] Gusev V, Kogan M and Perepukhov V. The similarity and aerodynamic measurements in transitional regime at hypersonic speeds. *Uchenyye Zapiski TsAGI*, Vol. 1, No. 1, pp. 24-31, 1970 (in Russian).

[6] Gusev V, Klimova T and Riabov V. The main regularities of aerodynamic characteristics changes in the transitional regimes of hypersonic flows. *Uchenyye Zapiski TsAGI*, Vol. 7, No. 3, pp. 47-57, 1976 (in Russian).

[7] Gusev V, Erofeev A, Klimova T, Perepukhov V, Riabov V and Tolstykh A. Theoretical and experimental investigations of flow over simple shape bodies by a hypersonic stream of rarefied gas. *Trudy TsAGI*, No. 1855, pp. 3-43, 1977 (in Russian).

[8] Riabov V. Aerodynamic applications of underexpanded hypersonic viscous jets. *Journal of Aircraft*, Vol. 32, No. 3, pp. 471-479, 1995.

[9] Riabov V. Comparative similarity analysis of hypersonic rarefied gas flows near simple-shape bodies. *Journal of Spacecraft and Rockets*, Vol. 35, No. 4, pp. 424-433, 1998.

[10] Riabov V. Aerodynamics of two side-by-side plates in hypersonic rarefied-gas flows. *Journal of Spacecraft and Rockets*, Vol. 39, No. 6, pp. 910-916, 2002.

[11] Riabov V. Numerical study of hypersonic rarefied-gas flows about a torus. *Journal of Spacecraft and Rockets*, Vol. 36, No. 2, pp. 293-296, 1999.

[12] Ivanov S and Yanshin A. Forces and moments acting on bodies rotating about a symmetry axis in a free molecular flow, *Fluid Dynamics*, Vol. 15, No. 3, pp. 449-453, 1980.

[13] Riabov V. Aerodynamics of a spinning cylinder in rarefied gas flows. *Journal of Spacecraft and Rockets*, Vol. 36, No. 3, pp. 486-488, 1999.

[14] Bird G. *The DS2G program user's guide, version 3.2*. G. A. B. Consulting Pty Ltd., Killara, New South Wales, Australia, pp. 1-56, 1999.

[15] Riabov V. Heat transfer on a hypersonic sphere with diffuse rarefied-gas injection. *Journal of Spacecraft and Rockets*, Vol. 41, No. 4, pp. 698-703, 2004.

[16] Botin A, Gusev V, Provotorov V, Riabov V and Chernikova L. Study of the influence of physical processes on heat transfer toward the blunt bodies in flows with small Reynolds numbers. *Trudy TsAGI*, Issue 2436, pp. 134-144, 1990 (in Russian).

[17] Nomura S. On a determination of heat flux at a critical stagnation point of a blunt body in hypersonic flow at small Reynolds numbers. *AIAA Journal*, Vol. 22, No. 7, 1984.

[18] Gusev V and Nikolsliy Yu. Experimental study of heat transfer at a critical stagnation point of a sphere in hypersonic rarefied-gas flow. *Uchenyye Zapiski TsAGI*, Vol. 2, No. 1, 1971 (in Russian).

[19] Klimova T and Chernikova L. A study of heat transfer in hypersonic rarefied-gas flow. *Rarefied Gas Dynamics. Proc. 6th All-Union Conference on RFG*. Novosibirsk, 1980 (in Russian).

[20] Riabov V and Provotorov V. The structure of multicomponent nonequilibrium viscous shock layers. *AIAA Paper*, No. 94-2054, pp. 1-8, 1994.

[21] Riabov V. Nonequilibrium and rarefaction effects in the hypersonic multicomponent viscous shock layers. *Proc. 24th International Congress of the Aeronautical*

Sciences. Paper 34. Yokohama, Japan, September 3-8, 2004.

[22] Molodtsov V and Riabov V. Investigation of the structural features of rarefied gas flows about a sphere using Navier-Stokes equations. *Proc. 13th International Symposium on Rarefied Gas Dynamics*, Novosibirsk, Vol. 1, pp. 535-541, 1985.

[23] Botin A. A Study of local heat transfer to the spherical surface with gas injection at small Reynolds numbers. *Uchenyye Zapiski TsAGI*, Vol. 18, No. 5, pp. 41-47, 1987 (in Russian).

[24] Riabov V. Interference between two side-by-side cylinders in hypersonic flows, *AIAA Paper*, No. 3297, pp. 1-6, 2002.

[25] Hall J and Le A. Aerocapture trajectories for spacecraft with large, towed ballutes. *AAS/AIAA Space Flight Mechanics Meeting*, Paper AAS 01-235, 2001.

[26] Gnoffo P and Anderson B. Computational analysis of towed ballute interactions, *AIAA Paper*, No. 2997, 2002.

[27] Moss J. DSMC Simulations of ballute aerothermodynamics under hypersonic rarefied conditions, *AIAA Paper*, No. 4949, 2005.

[28] McIntyre T, Lourel I, et al. Experimental expansion tube study of the flow over a toroidal ballute. *Journal of Spacecraft and Rockets*, Vol. 41, No. 5, pp. 716-725, 2004.

[29] Lourel I, Morgan R, et al. The effect of dissociation on chocking of ducted flows, *AIAA Paper*, No. 2894, 2002.

[30] Riabov V. Simulation techniques in hypersonic aerothermodynamics. *Proc. 23rd International Congress of the Aeronautical Sciences*. Paper 181. Toronto, Canada, September 8-13, 2002.